The Journal of Physical Chemistry Letters

pubs.acs.org/JPCL Letter

Data-Driven Photoluminescence Tuning in Eu^{2+}-Doped Phosphors

Shunqi Lai, Ming Zhao, Jianwei Qiao, Maxim S. Molokeev, and Zhiguo Xia*

Cite This: J. Phys. Chem. Lett. 2020, 11, 5680−5685 Read Online

ACCESS | Metrics & More | Article Recommendations | Supporting Information

ABSTRACT: Discovery of rare earth phosphors has generally relied on the chemical intuition and time-intensive trial-and-error synthesis; therefore, finding new materials assisted by data-driven computations is urgent. Herein, we utilize a regression model to predict the emission wavelengths of Eu^{2+}-doped phosphors by revealing the relationships between the crystal structure and luminescence property. The emission wavelengths of $[Rb_{(1-x)}K_{(x)}]_3LuSi_2O_7{:}Eu^{2+}$ ($0 \le x \le 1$) phosphors, as examples for the data-driven photoluminescence tuning, are successfully predicted on the basis of the existing data of only eight systems, also consistent with the experimental results. These phosphors can be excited by blue light and exhibit broad-band red and near-infrared emission ranging from 619 to 737 nm. These findings in Eu^{2+}-doped silicate phosphors indicate that data-driven computations through the regression mode would have bright application in discovering novel phosphors with a target emission wavelengths.

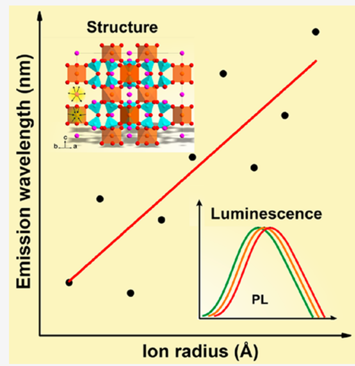

Phosphor-converted light-emitting diodes (*pc*-LEDs) have become the next-generation lighting source due to high efficiency, low energy consumption, long lifetime, and environmental compatibility.[1−3] Until now, *pc*-LED technology has been widely used in many fields, such as general lighting, automotive lighting, display backlight, medical diagnostics, plant lighting, and so on.[4−7] Therefore, it is critical to develop phosphors with appropriate emission wavelengths, and many strategies have been adopted to discover new phosphors, such as trial-and-error searching in different crystal structure databases, combinatorial chemistry screening with high throughput experimentation, chemical unit cosubstitution based on a structural model, or single-particle diagnosis approach.[8,9] Thus, many novel phosphors with various emission wavelengths have been discovered through those approaches.[10−12] Nevertheless, these methods are largely conducted through painstaking experiments in an Edisonian fashion, which require the abundant experience and massive experimentation.[9] Driven by the rapid development of computers, the advancement of algorithms, and the explosion of experimental material databases, machine learning techniques have become powerful tools for materials discovery.[13,14] Recently, data-driven methodologies have been demonstrated to be successful in computational design and experimental identification for novel phosphors. Brgoch's group established a thermally robust phosphor $NaBaB_9O_{15}{:}Eu^{2+}$ with the assistance of machine learning and high-throughput density functional theory (DFT) calculations.[15] In addition, Wang et al. adopted a carefully targeted data-driven structure prediction and screening effort to discover a new phosphor, $Sr_2LiAlO_4{:}Eu^{2+}$, in the first Sr−Li−Al−O quaternary crystal system.[16] Data-driven methodology provides a convenient way to find novel phosphors; however, the core problem is to propose decision rules, which enable us to establish a mapping between measurable and easily accessible attributes of a system and its properties.[17]

Over the last years, Eu^{2+}-doped compounds have been extensively investigated for phosphors in pc-LEDs. In most cases, the observed Eu^{2+} luminescence arises from the parity-allowed transition between the $4f^7(^8S_{7/2})$ ground state and the $4f^6(^7F)5d^1$ excited state.[7,8] The emission energies of this transition show a high sensitivity toward the local coordination environment, that is to say, by changing the crystal structure, the emission colors of Eu^{2+}-doped phosphors would be changed and also predicted. The relationship between crystal structure and luminescence properties is still a holy grail for the phosphor materials discovery.[18,19] Nevertheless, study of structure−property association is a challenge owing to the multiparameter and complexity of the task. Ab initio theoretical calculations can predict the structure−property relationship, but it has a heavy workload on account of the huge calculations and the special knowledge needs. Artificial intelligence (AI) can make easy predictions if there is an adequate database.[20,21] Machine learning acting as a hot tool usually demands more examples, in contrast to the limited amounts of phosphor materials with particular interests.[22] However, regression analysis, as another way, refers to a set of statistical processes for estimating the relationships between a

Received: May 13, 2020
Accepted: June 22, 2020
Published: June 22, 2020

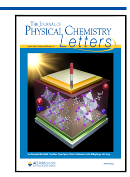

https://dx.doi.org/10.1021/acs.jpclett.0c01471
J. Phys. Chem. Lett. 2020, 11, 5680−5685

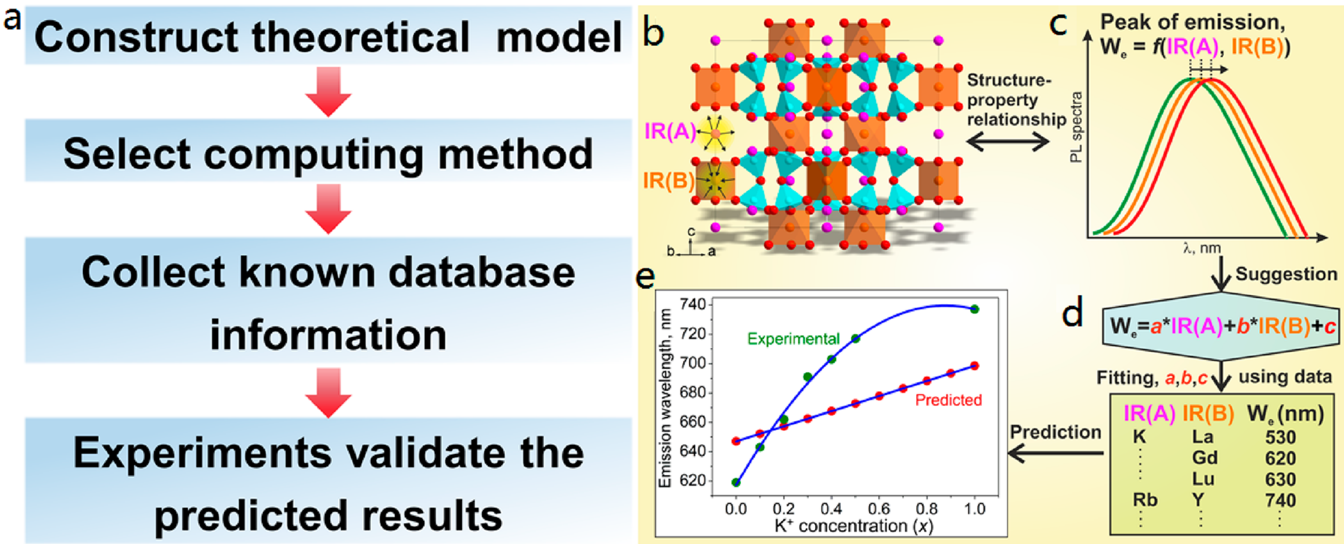

Figure 1. (a) Full data-driven steps by regression analysis. (b, c) Crystal structure model of $A_3BSi_2O_7$ and the relationship between structure and luminescence property. (d) Assumed formula and the related database for prediction. (e) Theoretically predicted and experimentally observed emission wavelengths of $R_{1-x}K_xLSO:0.01Eu^{2+}$ ($0 \leq x \leq 1$) phosphors.

dependent variable, called the "outcome variable", and one or more independent variables, also called "predictors", "covariates", or "features".[23] This analysis is not so restricted to the amounts of samples and can be easily applied to a database of 13−100 samples. There are many types of regression analysis, including simple regression, multiple regression, logistic regression, and so on.[24] For instance, Pilania et al. successfully used a kernel ridge regression model to predict the electronic properties.[17] Here, we use simple regression analysis to establish the relationship of crystal structure and luminescence properties to predict the emission wavelength of the unknown phosphors.

Recently, we discovered a series of Eu^{2+}-doped $A_3BSi_2O_7$-type (A = alkali metal ions; B = rare-earth metal ions) phosphors, including $K_3YSi_2O_7:Eu^{2+}$, $K_3LuSi_2O_7:Eu^{2+}$, and $Rb_3YSi_2O_7:Eu^{2+}$,[25−27] which can be excited by blue light and emit red or near-infrared light. The typical $A_3BSi_2O_7$ compounds have similar structures and the local structure only can be affected by the A and B ions. Hence, two parameters of ion radius A and B need to be varied during the process of modeling, which greatly reduces the modeling difficulty. In this work, the luminescence properties of some reported phosphors in $A_3BSi_2O_7:Eu^{2+}$ families are chosen as the database, and regression analysis is used to establish a model that can predict the emission wavelengths of the class of phosphors. The solid solution phosphors formed by $K_3LuSi_2O_7:Eu^{2+}$ and $Rb_3LuSi_2O_7:Eu^{2+}$ are chosen to verify the accuracy of the model. The photoluminescence tuning of $[Rb_{(1-x)}K_{(x)}]_3LuSi_2O_7:Eu^{2+}$ ($0 \leq x \leq 1$) (abbreviated as $R_{1-x}K_xLSO:Eu^{2+}$) is accordant with the results predicted by simple regression analysis. In addition, all the phosphors exhibit broad red to near-infrared emission band under blue light excitation, which can be applied to the new lighting source. The results suggest that simple regression analysis is potentially a good method to predict the emission wavelength of unknown phosphors.

Since there are only eight systems of original data, unknown parameters in the calculation model must be kept as small as possible to avoid overfitting. Here, the linear regression model is used for prediction. The experimental details and the construction of the regression model have been described in the Supporting Information, where correlation of the data from a sample and the estimated linear regression line for these data are discussed and demonstrated in Figure S1. Furthermore, the data-driven steps via the regression model for prediction are shown in Figure 1a. Here, we use linear regression analysis to establish the relationship of structure and luminescence properties to predict the emission wavelength of a class of phosphors $A_3BSi_2O_7:Eu^{2+}$. There are only two varied parameters, ion radii (Å) of A and B for the $A_3BSi_2O_7:Eu^{2+}$ phosphors, where ion radii of A and B refer to x and y refers to the emission wavelength, as demonstrated by the crystal structure model and emission spectra of $A_3BSi_2O_7:Eu^{2+}$ phosphors (Figure 1b,c). Due to those, we obtain a linear function of ion radii:

$$W_e = a \times IR(A) + b \times IR(B) + c \quad (1)$$

where W_e refers to the emission wavelength and a, b, and c refer to some unknown constants that should be defined (Figure 1d). We used the information about the wavelength emission of several known $A_3BSi_2O_7:Eu^{2+}$ phosphors (Table 1) to make the fitting, and the emission spectra of as-prepared $Rb_3GdSi_2O_7:Eu^{2+}$, $Rb_3LuSi_2O_7:Eu^{2+}$, $K_3LaSi_2O_7:Eu^{2+}$, $K_3GdSi_2O_7:Eu^{2+}$, and $K_3ScSi_2O_7:Eu^{2+}$ are given in Figure S2. The excitation wavelength varies from 330 to 450 nm, but we

Table 1. Excitation and Emission Wavelengths of $A_3BSi_2O_7:Eu^{2+}$ Phosphors Obtained by Experiments and Previous Work

materials	excitation, nm	emission, nm
$K_3LaSi_2O_7$	365	530
$K_3YSi_2O_7$	450	620[25]
$K_3GdSi_2O_7$	400	630
$K_3LuSi_2O_7$	450	740[26]
$K_3ScSi_2O_7$	450	740
$Rb_3YSi_2O_7$	450	622[27]
$Rb_3GdSi_2O_7$	330	550
$Rb_3LuSi_2O_7$	450	619

https://dx.doi.org/10.1021/acs.jpclett.0c01471
J. Phys. Chem. Lett. 2020, 11, 5680−5685

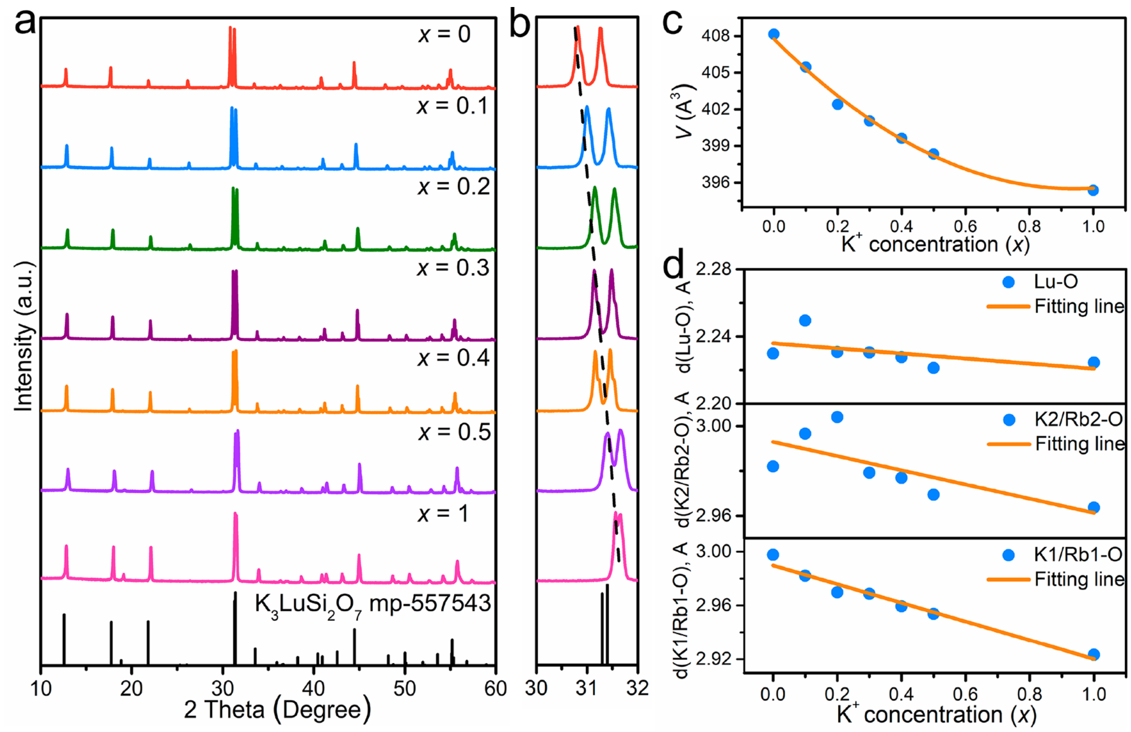

Figure 2. (a) Standard pattern (obtained from Materials Project, mp-557543) of $K_3LuSi_2O_7$ and as-measured XRD patterns of $R_{1-x}K_xLSO$:0.01Eu^{2+} ($0 \leq x \leq 1$). (b) Selected diffraction peaks near 31° of $R_{1-x}K_xLSO$:0.01Eu^{2+} ($0\leq x \leq 1$). (c) Cell volume $V(x)$ dependence of K^+ concentration. (d) Dependence of the average bond length of Lu, K1/Rb1, and K2/Rb2 in $R_{1-x}K_xLSO$:0.01Eu^{2+} ($0 \leq x \leq 1$).

did not focus on it and almost the same prediction results are found when we use the same excitation wavelength corresponding to the emission wavelength for the prediction. After regression analysis, the equation appeared to be

$$W_e = 2364.586 - 644.061 \times \mathrm{IR(A)} - 775.554 \times \mathrm{IR(B)} \tag{2}$$

Therefore, the eq 2 was used to predict the emission of $[Rb_{(1-x)}K_{(x)}]_3LuSi_2O_7$:$Eu^{2+}$ and theoretically predicted and experimentally observed emission wavelengths are depicted in Figure 1e. The residual between expected and all observed data was in the range 5−50 nm, and the maximum value seems to be not very good. This may be due to the fact that what we predicted is a linear curve, while the experimental results prefer a quadratic curve that needed more original data for the prediction. However, one can see that the trend in Figure 1e was revealed very well, and similar trends can be also obtained for any compound with chemical formula of $A_3BSi_2O_7$:Eu^{2+}. Moreover, the analysis of eq 2 revealed the following: (1) The increasing of A and B ionic radii should lead to a blue shift of wavelength emission. For example, most Cs-containing or La-containing compounds should lead to a blue shift. (2) By contrast, the decrease of the radii of A and B ions should lead to a red shift. For example, Na-containing or Lu-containing compounds should lead to a red shift. (3) The A ion has a bigger influence on wavelength than the B ion, because usually ionic radii of A vary in the range 1.24−1.78 Å (Na−Cs ions) whereas B ions vary in the more narrow range of 1.032−1.216 Å (Lu−La ions) and the absolute value is smaller; however, the difference between the coefficients of $a = -644.061$ and $b = -775.554$ is not very big in the multiplicative model. Thus, the simple formula with only two variables revealed the global trends and structure−property relationships, which are very important in materials science.

To further check the rationality of the data-driven photoluminescence tuning revealed by the regression model and explain the possible mechanisms, the phase structures and luminescence properties of $R_{1-x}K_xLSO$:0.01Eu^{2+} phosphors have been investigated in detail. Figure 2a shows the XRD patterns of the as-prepared $R_{1-x}K_xLSO$:0.01Eu^{2+} solid solution, which can be well indexed to the reported pattern of a hexagonal ($P6_3/mmc$) phase $K_3LuSi_2O_7$. Due to the smaller ionic radius of the K^+ ion than the Rb^+ ion, the enlarged diffraction peaks from 2θ = 30°−32° of $R_{1-x}K_xLSO$:0.01Eu^{2+} samples continuously shift toward larger angles with the increase of x compared with the position of $Rb_3LuSi_2O_7$:0.01Eu^{2+} (Figure 2b), indicating there is a lattice shrinkage with substituting Rb^+ by K^+. Moreover, further Rietveld refinement of the series of $R_{1-x}K_xLSO$:0.01Eu^{2+} has been performed, and the main parameters are shown in Table S1. $K_3LuSi_2O_7$ was taken as the starting model for Rietveld refinement.[28] The sites of K^+ ions are occupied by K^+/Rb^+ ions according to the suggested chemical formula. Minor impurity phases of Lu_2O_3 were found at about 0.8−1.5%, which would have no impact on the luminescence properties of these phosphors. Furthermore, the variations of the cell volumes and bond lengths of each sample are shown in Figure 2c,d, and coordinates of atoms and main bond lengths are shown in Tables S2 and S3, respectively. Obviously, the relative content of K and Rb has little effect on the average bond lengths of Lu−O, while the average bond lengths of K1/Rb1−O and K2/Rb2−O decrease almost linearly as the increase of K^+ concentration, which indicates K^+ ions have definitely entered the Rb^+ lattice to form a solid solution. It is further confirmed by the cell volume (V) of $R_{1-x}K_xLSO$:0.01Eu^{2+} samples, which decreases linearly with x in good agreement with the fact that the K^+ ion has a smaller ionic radius than the Rb^+ ion obeying the Vegard's rule.[29]

https://dx.doi.org/10.1021/acs.jpclett.0c01471
J. Phys. Chem. Lett. 2020, 11, 5680−5685

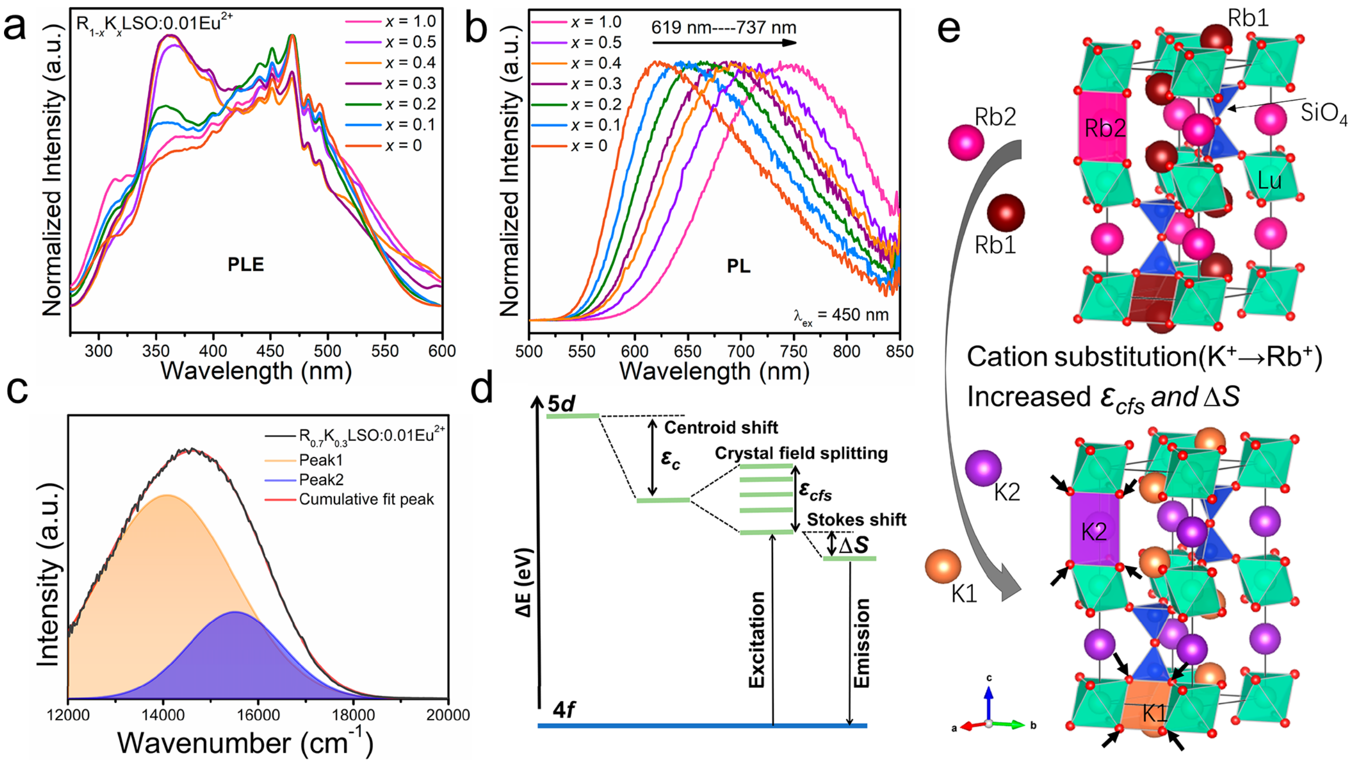

Figure 3. Normalized PLE (a) and PL (b) spectra of as-prepared $R_{1-x}K_xLSO:0.01Eu^{2+}$ ($0 \le x \le 1$). (c) Gaussian fitting curves of the emission spectrum of $R_{1-x}K_xLSO:0.01Eu^{2+}$ ($x = 0.3$). (d) Schematic energy level diagram for Eu^{2+} ions in RKLSO:$0.01Eu^{2+}$ phosphors showing the centroid shift ε_c, the crystal field splitting effect ε_{cfs}, and the Stokes shift ΔS. (e) Schematic diagram of the K^+ substitution process leading to the variation of the local structures.

The crystal structures of $Rb_3LuSi_2O_7$ display an atom configuration similar to that of $K_3LuSi_2O_7$. As seen in Figure 1b and Figure S3, all the fundamental frameworks are constructed by LuO_6 octahedra and Si_2O_7 units via vertex-sharing. K^+/Rb^+ displays the same coordination form in the channel composed by LuO_6 octahedra and Si_2O_7 units, with sites having 9-fold (K1/Rb1) and 6-fold (K2/Rb2) coordination in the unit cell and two kinds of polyhedrons connected to each other by sharing the same vertexes and edges. In $K_3LuSi_2O_7$, the main doping mechanism is ascribed to the synergetic effect of Lu → Eu and K2 → Eu replacements, as discussed before.[25−27] Due to the similar crystal structure and the same cationic coordination environment in $R_{1-x}K_xLSO:Eu^{2+}$ samples, the main doping mechanism of Eu ion remains unchanged, which is further illustrated in the following analysis of luminescence performance. This same crystal structure and Eu^{2+} occupancy in $A_3BSi_2O_7:Eu^{2+}$ phosphors guarantees the results obtained from the regression model.

As shown in Figure 3a, the PLE spectra of $R_{1-x}K_xLSO:0.01Eu^{2+}$ samples possess broad-band excitation in the region of 250−600 nm and these phosphors are suitable for the commercial blue chips. The excitation peaks position and shape are almost unchanged with increasing substituted cation concentration in $R_{1-x}K_xLSO:0.01Eu^{2+}$ samples, except for slightly increasing of bandwidth. Upon 450 nm excitation, the PL spectra of $R_{1-x}K_xLSO:0.01Eu^{2+}$ exhibit a consecutive red shift from orange-red light to near-infrared light with the increase of K^+ concentration as shown in Figure 3b. As is shown in Table S4, the emission peak shifts from 619 to 737 nm. Moreover, all PL spectra can be decomposed into two Gaussian curves, which indicates that Eu^{2+} ions occupy two different sites, as shown in Figure 3c. The photoluminescence decay lifetime is an efficient method to analyze the site occupation in the phosphor materials. All the photoluminescence decay curves of [$K^+ \rightarrow Rb^+$] phosphors obey the biexponential model (Figure S4), which further certifies that Eu^{2+} occupies two cation sites (K2/Rb2 and Lu sites), as discussed before. The calculated lifetime values changed gradually, which is related to the energy transfer among two Eu^{2+} centers.

To better understand the large-scale emission tuning in $R_{1-x}K_xLSO:0.01Eu^{2+}$ phosphors, the local lattice environment around Eu^{2+} is used to reveal the intrinsic mechanism. The schematic energy level diagram for Eu^{2+} ions in RKLSO:$0.01Eu^{2+}$ phosphors and the schematic diagram of K^+ substitution process are shown in Figure 3d,e. For the $R_{1-x}K_xLSO:0.01Eu^{2+}$ phosphor, the centroid shift has a weak effect on the red shift because of the low covalence between Eu^{2+} and O^{2-} ions. Considering the sensitivity of Eu^{2+} ions to the crystal field environment, the cation substitution of K^+ for Rb^+ would directly influence the luminescence properties. When Rb^+ ions are substituted by K^+ ions, the K^+ ions randomly occupy the Rb^+ sites, including the neighboring Rb^+ sites around the Eu^{2+} ions. The local structural variation caused by cation substitution around the luminescent centers would definitely influence the crystal field strength.[27] On the basis of crystal field theory, the type of polyhedron and bond length between the central cation and its ligands are important factors in determining the crystal field strength of the Rb^+ sites occupied by K^+ ions. In general, the crystal field strength (D_q) could be identified via the expression:[30]

https://dx.doi.org/10.1021/acs.jpclett.0c01471
J. Phys. Chem. Lett. 2020, 11, 5680−5685

$$D_q = \frac{Ze^2r^4}{6R^5} \quad (3)$$

where Z is the charge or valence of the anion, e is the electron charge, r refers to the radius of the d wave function, and R is the bond length between the central cation and its ligands. The D_q value is inversely proportional to the R value. Theoretically, the substitution of Rb^+ by K^+ would generate an increased crystal field splitting due to the decreased R value, which reduces the energy of the lowest 5d level. The emission spectrum is determined by the lowest 5d energy level and Stokes shift. Herein, we further estimated the Stokes shift from the spectra in Figure 3a,b, which is twice the energy difference between the intersection point of excitation and emission spectra and the peak of the emission spectra.[31,32] It increases from 3586 to 5152 cm^{-1} with the increasing of K^+ concentration. Since the Stokes shift is greatly influenced by the rigidity of crystal structure, the substitution of K^+ ions could impair the rigidity, leading to the gradually increasing Stokes shift, which results in the spectral red shift.[33,34] Therefore, we can reasonably conclude that the red shift is caused by the combined effect of Stokes shift and crystal field strength.

When we recall the comparison between the maximum emission wavelengths of the experiment and the prediction depicted in Figure 1e, one can find that the increasing trend is almost the same as predicted by the simple regression analysis. These results suggest that it is a potentially good way to predict the emission wavelength of unknown phosphors. It is interesting that the simple model and easy calculations could give us predictive conclusions. More complex compounds not only for the solid solution but also the isostructural compounds can be also treated by using this model with the help of CIE coordinates (x, y), Ra (color rendering index), and so on. Therefore, experimentally investigating this series of phosphors will provide much support to the regression analysis as a tool for identifying the emission wavelength of new inorganic phosphors.

In summary, a calculation model based on the connection between crystal structure and luminescence properties in $A_3BSi_2O_7:Eu^{2+}$ (A = alkali metal ions; B = rare-earth metal ions) is used to identify the emission wavelength of unknown phosphors. With the assistance of a simple regression analysis, the increasing/decreasing of A and B ion radii should lead to a blue/red shift of wavelength emission. We established a linear function of ion radii to predict the emission wavelengths of $R_{1-x}K_xLSO:0.01Eu^{2+}$ phosphors, and the emission peaks displays the shift from 619 to 737 nm with the x increasing from 0 to 1. The red shift of emission spectra is attributed to the combined effect of the increased crystal field splitting and the increased Stokes shift. These results support that regression analysis is an indispensable method to direct the search for new rare-earth phosphors even if the amount of samples is very small. All the phosphors show the red and near-infrared emission under the excitation of blue light, indicating potentials in new lighting sources, and the methods used have a good directivity for the future application of regression analysis for other functional materials.

■ ASSOCIATED CONTENT

Supporting Information

The Supporting Information is available free of charge at https://pubs.acs.org/doi/10.1021/acs.jpclett.0c01471.

Experimental section and description of the regression model; linear regression of sample data; PLE and PL spectra of as-prepared $Rb_3GdSi_2O_7:Eu^{2+}$, $Rb_3LuSi_2O_7:Eu^{2+}$, $K_3LaSi_2O_7:Eu^{2+}$, $K_3GdSi_2O_7:Eu^{2+}$, and $K_3ScSi_2O_7:Eu^{2+}$; the coordination of metal cations in $Rb_3LuSi_2O_7$; photoluminescence decay curves of $R_{1-x}K_xLSO:0.01Eu^{2+}$; main parameters of refinement, coordinates of atoms, main bond lengths, and specific emission wavelength of the mentioned samples (PDF)

■ AUTHOR INFORMATION

Corresponding Author

Zhiguo Xia − *State Key Laboratory of Luminescent Materials and Devices, Guangdong Provincial Key Laboratory of Fiber Laser Materials and Applied Techniques, School of Materials Science and Engineering, South China University of Technology, Guangzhou 510641, China; The Beijing Municipal Key Laboratory of New Energy Materials and Technologies, School of Materials Sciences and Engineering, University of Science and Technology Beijing, Beijing 100083, China;* orcid.org/0000-0002-9670-3223; Email: xiazg@scut.edu.cn

Authors

Shunqi Lai − *State Key Laboratory of Luminescent Materials and Devices, Guangdong Provincial Key Laboratory of Fiber Laser Materials and Applied Techniques, School of Materials Science and Engineering, South China University of Technology, Guangzhou 510641, China*

Ming Zhao − *State Key Laboratory of Luminescent Materials and Devices, Guangdong Provincial Key Laboratory of Fiber Laser Materials and Applied Techniques, School of Materials Science and Engineering, South China University of Technology, Guangzhou 510641, China; The Beijing Municipal Key Laboratory of New Energy Materials and Technologies, School of Materials Sciences and Engineering, University of Science and Technology Beijing, Beijing 100083, China*

Jianwei Qiao − *State Key Laboratory of Luminescent Materials and Devices, Guangdong Provincial Key Laboratory of Fiber Laser Materials and Applied Techniques, School of Materials Science and Engineering, South China University of Technology, Guangzhou 510641, China; The Beijing Municipal Key Laboratory of New Energy Materials and Technologies, School of Materials Sciences and Engineering, University of Science and Technology Beijing, Beijing 100083, China*

Maxim S. Molokeev − *Laboratory of Crystal Physics, Kirensky Institute of Physics, Federal Research Center KSC SB RAS, Krasnoyarsk 660036, Russia; Siberian Federal University, Krasnoyarsk 660041, Russia; Department of Physics, Far Eastern State Transport University, Khabarovsk 680021, Russia*

Complete contact information is available at:
https://pubs.acs.org/10.1021/acs.jpclett.0c01471

Notes

The authors declare no competing financial interest.

■ ACKNOWLEDGMENTS

The present work was supported by the National Natural Science Foundations of China (Grant No. 51972118, 51961145101 and 51722202), Fundamental Research Funds for the Central Universities (D2190980), Guangzhou Science & Technology Project (202007020005), Guangdong Provincial Science & Technology Project (No. 2018A050506004), and the Local Innovative and Research Teams Project of Guangdong Pearl River Talents Program (2017BT01X137). This work is also funded by RFBR according to the research project No. 19-52-80003.

■ REFERENCES

(1) Reineke, S. Complementary LED Technologies. *Nat. Mater.* **2015**, *14*, 459−462.

(2) Xia, Z.; Xu, Z.; Chen, M.; Liu, Q. Recent Developments in the New Inorganic Solid-State LED Phosphors. *Dalton Trans.* **2016**, *45*, 11214−11232.

(3) Wang, L.; Xie, R.-J.; Suehiro, T.; Takeda, T.; Hirosaki, N. Down-Conversion Nitride Materials for Solid State Lighting: Recent Advances and Perspectives. *Chem. Rev.* **2018**, *118*, 1951−2009.

(4) Zhao, M.; Liao, H.; Molokeev, M. S.; Zhou, Y.; Zhang, Q.; Liu, Q.; Xia, Z. Emerging Ultra-Narrow Band Cyan-Emitting Phosphor for White LEDs with Enhanced Color Rendition. *Light: Sci. Appl.* **2019**, *8*, 38−46.

(5) Hoppe, H. Recent Developments in the Field of Inorganic Phosphors. *Angew. Chem., Int. Ed.* **2009**, *48*, 3572−3582.

(6) Tang, Z.; Zhang, Q.; Cao, Y.; Li, Y.; Wang, Y. Eu^{2+}-Doped Ultra-Broadband VIS-NIR Emitting Phosphor. *Chem. Eng. J.* **2020**, *388*, 124231−124239.

(7) Mao, Z.; Li, J.; Wang, D. Dual-Responsive $Sr_2SiO_4:Eu^{2+}$-$Ba_3MgSi_2O_8:Eu^{2+}$, Mn^{2+} Composite Phosphor to Human Eyes and Plant Chlorophylls Applications for General Lighting and Plant Lighting. *Chem. Eng. J.* **2016**, *284*, 1003−1007.

(8) Xia, Z.; Liu, Q. Progress in Discovery and Structural Design of Color Conversion Phosphors for LEDs. *Prog. Mater. Sci.* **2016**, *84*, 59−117.

(9) Li, S.; Xie, R. Critical Review—Data-Driven Discovery of Novel Phosphors. *ECS J. Solid State Sci. Technol.* **2020**, *9*, 016013−016019.

(10) Qiao, J.; Zhao, J.; Xia, Z. A Review on the Eu^{2+} Doped β-$Ca_3(PO_4)_2$-Type Phosphors and the Sites Occupancy for Photoluminescence Tuning. *Opt. Mater.: X.* **2019**, *1*, 100019−100027.

(11) Cheng, C.; Ning, L.; Ke, X.; Molokeev, M. S.; Wang, Z.; Zhou, G.; Chuang, Y.; Xia, Z. Designing High-Performance LED Phosphors by Controlling the Phase Stability via a Heterovalent Substitution Strategy. *Adv. Opt. Mater.* **2020**, *8*, 1901608−1901616.

(12) Takeda, T.; Hirosaki, N.; Funahshi, S.; Xie, R. Narrow-Band Green-Emitting Phosphor $Ba_2LiSi_7AlN_{12}:Eu^{2+}$ with High Thermal Stability Discovered by a Single Particle Diagnosis Approach. *Chem. Mater.* **2015**, *27*, 5892−5898.

(13) Zhuo, Y.; Hariyani, S.; Armijo, E.; Abolade Lawson, Z.; Brgoch, J. Evaluating Thermal Quenching Temperature in Eu^{3+}-Substituted Oxide Phosphors via Machine Learning. *ACS Appl. Mater. Interfaces* **2020**, *12*, 5244−5250.

(14) Butler, K.; Davies, D.; Cartwright, H.; Isayev, O.; Walsh, A. Machine Learning for Molecular and Materials Science. *Nature* **2018**, *559*, 547−555.

(15) Zhuo, Y.; Mansouri Tehrani, A.; Oliynyk, A. O.; Duke, A. C.; Brgoch, J. Identifying an Efficient, Thermally Robust Inorganic Phosphor Host via Machine Learning. *Nat. Commun.* **2018**, *9*, 4377−4387.

(16) Wang, Z.; Ha, J.; Kim, Y. H.; Im, W.; McKittrick, J.; Ong, S. Mining Unexplored Chemistries for Phosphors for High-Color-Quality White-Light-Emitting Diodes. *Joule.* **2018**, *2*, 914−926.

(17) Pilania, G.; Wang, C.; Jiang, X.; Rajasekaran, S.; Ramprasad, R. Accelerating Materials Property Predictions Using Machine Learning. *Sci. Rep.* **2013**, *3*, 2810−2816.

(18) Ding, X.; Cao, H.; Mu, Y.; Zhu, G.; Xia, D. The Structure and Photoluminescence Properties of A Novel Orange Emission Phosphor $Ba_3Sc_{1.9}Al_{0.1}B_4O_{12}$: Eu^{2+} Excited by NUV Light. *Opt. Mater.* **2019**, *92*, 195−205.

(19) Wei, Y.; Gao, Z.; Liu, S.; Chen, S.; Xing, G.; Wang, W.; Dang, P.; Li, G. Highly Efficient Green-to-Yellowish-Orange Emitting Eu^{2+}-Doped Pyrophosphate Phosphors with Superior Thermal Quenching Resistance for w-LEDs. *Adv. Opt. Mater.* **2020**, *8*, 1901859−1901872.

(20) Pokluda, J.; Cerny, M.; Šob, M.; Umeno, Y. Ab Initio Calculations of Mechanical Properties: Methods and Applications. *Prog. Mater. Sci.* **2015**, *73*, 127−158.

(21) Reid, F.; Duan, C.; Zhou, H. Crystal−field Parameters From Ab Initio Calculations. *J. Alloys Compd.* **2009**, *488*, 591−594.

(22) Yang, F.; Wang, Y.; Jiang, X.; Lin, B.; Lv, R. Optimized Multimetal Sensitized Phosphor for Enhanced Red Up-Conversion Luminescence by Machine Learning. *ACS Comb. Sci.* **2020**, *22*, 285−296.

(23) Aggarwal, R.; Ranganathan, P. Common Pitfalls in Statistical Analysis: Linear Regression Analysis. *Perspect Clin. Res.* **2017**, *8*, 100−102.

(24) Duleba, A.; Olive, D. Regression Analysis and Multivariate Analysis. *Semin. Reprod. Med.* **1996**, *14*, 139−153.

(25) Qiao, J.; Amachraa, M.; Molokeev, M. S.; Chuang, Y.; Ong, S.; Zhang, Q.; Xia, Z. Engineering of $K_3YSi_2O_7$ To Tune Photoluminescence with Selected Activators and Site Occupancy. *Chem. Mater.* **2019**, *31*, 7770−7778.

(26) Qiao, J.; Zhou, G.; Zhou, Y.; Zhang, Q.; Xia, Z. Divalent Europium-Doped Near-Infrared-Emitting Phosphor for Light-Emitting Diodes. *Nat. Commun.* **2019**, *10*, 5267−5274.

(27) Qiao, J.; Ning, L.; Molokeev, M. S.; Chuang, Y.; Zhang, Q.; Kenneth, R. P.; Xia, Z. Site-Selective Occupancy of Eu^{2+} Toward Blue-Light-Excited Red Emission in a $Rb_3YSi_2O_7$:Eu Phosphor. *Angew. Chem., Int. Ed.* **2019**, *58*, 11521−11526.

(28) Vidican, I.; Smith, M. D.; zur Loye, H. C. Crystal Growth, Structure Determination, and Optical Properties of New Potassium-Rare-Earth Silicates $K_3RESi_2O_7$ (RE= Gd, Tb, Dy, Ho, Er, Tm, Yb, Lu). *J. Solid State Chem.* **2003**, *170*, 203−210.

(29) Dang, P.; Li, G.; Liang, S.; Lian, H.; Lin, J. Multichannel Photoluminescence Tuning in Eu-Doped Apatite Phosphors via Coexisting Cation Substitution, Energy Transfer and Valence Mixing. *J. Mater. Chem. C* **2019**, *7*, 5975−5987.

(30) Liu, Y.; Zhang, J.; Zhang, C.; Xu, J.; Liu, G.; Jiang, J.; Jiang, J. $Ba_9Lu_2Si_6O_{24}:Ce^{3+}$: An Efficient Green Phosphor with High Thermal and Radiation Stability for Solid-State Lighting. *Adv. Opt. Mater.* **2015**, *3*, 1096.

(31) Wang, S.; Song, Z.; Kong, Y.; Liu, Q. Relationship of Stokes Shift with Composition and Structure in Ce^{3+}/Eu^{2+}-doped Inorganic Compounds. *J. Lumin.* **2019**, *212*, 250−263.

(32) Qiu, Z.; Lian, H.; Shang, M.; Lian, S.; Lin, J. The Structural Evolution and Spectral Blue Shift of Solid Solution Phosphors $Sr_{3-m}Ca_mB_2O_6:Eu^{2+}$. *CrystEngComm* **2016**, *18*, 4597−4603.

(33) Ji, H.; Wang, L.; Molokeev, M.; Hirosaki, N.; Xie, R.; Huang, Z.; Xia, Z.; Kate, O.; Liu, L.; Atuchin, V. Structure Evolution and Photoluminescence of $Lu_3(Al,Mg)_2(Al,Si)_3O_{12}:Ce^{3+}$ Phosphors: New Yellow-Color Converters for Blue LED-Driven Solid State Lighting. *J. Mater. Chem. C* **2016**, *4*, 6855−6863.

(34) Daicho, H.; Shinomiya, Y.; Enomoto, K.; Nakano, A.; Sawa, H.; Matsuishi, S.; Hosono, H. A Novel Red-Emitting $K_2Ca(PO_4)F:Eu^{2+}$ Phosphor with A Large Stokes Shift. *Chem. Commun.* **2018**, *54*, 884−887.